


Photocatalysis Hot Paper

Chromophore-Inspired Design of Pyridinium-Based Metal–Organic Polymers for Dual Photoredox Catalysis

Qingqing Zhang, Yunhe Jin,* Lin Ma, Yongqiang Zhang, Changgong Meng, and Chunying Duan*

Abstract: 2,4,6-Triphenylpyrylium (TPT^+) functions as a classic organic photocatalyst and exhibits a noteworthy absorption in the visible range, strongly oxidizing excited states, and a somewhat unstable structure. Inspired by the nuclear chromophore and dual catalysis strategy, herein, we report a universal photoredox platform constructed by TPT^+ -mimic bridging ligands and reductive metal ions on the basis of metal–organic supramolecular systems for various organic couplings and molecular oxygen activation under visible-light irradiation. Significant photoinduced electron transfer and ligand-to-metal charge-transfer events are both integrated and regulated by the spatial and kinetic confinement effects of the structurally confined microenvironments, effectively improving the efficiency of electron transfer and radical–radical coupling processes in photocatalysis. This package deal provides a promising way for the design of novel photocatalysts and the development of versatile and sustainable synthetic chemistry.

Introduction

Photoredox catalysis is becoming an important synthetic strategy in organic synthesis, enabling the conversion from solar power to chemical energy.^[1] Compared to traditional synthetic reactions, visible-light-driven photocatalytic reactions usually proceed in a green and sustainable way under mild conditions.^[2] Diverse homogeneous photocatalysts, mainly including Ru/Ir complexes and organic dyes, exhibit capacities to absorb optical radiation and initiate organic reactions with single-electron transfer (SET) or energy transfer (EnT).^[1c,3] Assembly of different kinds of functional groups on the backbone can synergistically modulate the oxidation and reduction potentials of a photocatalyst, but it is always difficult to regulate one without any effect on the other.^[4] Besides, most photochemical reactions undergo a

radical pathway, which allows direct radical–radical coupling of non-traditional nucleophile partners and confers access to a broad range of organic synthesis.^[5] In terms of the character of the radicals, such as an unstable nature, low concentration, and incidental self-quenching, it remains a significant challenge to promote the photoreaction efficiency of radical–radical coupling and widen the application of photocatalysis.^[6] In the past several years, the dual catalytic system, which merges photocatalysis and transition-metal catalysis, has been demonstrated to be a versatile platform for the development of synthetic photochemistry.^[7] Within this strategy, the photocatalyst uptakes light and reacts with organic substrates to deliver photogenerated species, and the metal catalyst further manipulates the active radical intermediates to complete chemical transformations. Meanwhile, low concentrations of catalyst intermediates result in limited efficiency of the crucial electron transfer between two catalytic cycles, restricting the further application of this system to a certain degree.

Well known as hybrid porous crystalline materials linked by coordination bonds, metal–organic supramolecular systems have emerged as a powerful tool to mimic and study natural photosynthetic systems.^[8] Both the distinct parts of metal–organic polymers (MOPs)-metal nodes and organic linkers can be easily tailored for photocatalysis owing to their modular nature; the highly ordered structures, large surface areas, and uniform pores or channels of MOPs contribute to the exposure of active sites and diffusion of substrates during catalytic reactions.^[9] Importantly, by constructing photo- and metal catalysts into one crystalline material, the dense distribution and tight connection of both catalytically active sites ensure the charge transport processes, such as ligand-to-metal charge transfer (LMCT), between each other occurs conveniently owing to the spatial confinement effect of MOPs. The kinetic confinement effect of structurally confined microenvironments of MOPs can dock and gather the unstable radical intermediates around catalytic sites, increase the relative concentrations and collision probabilities of radicals, and thus result in efficient radical–radical couplings.^[10] Therefore, establishing a universal platform that depends on MOP materials and a dual catalysis strategy will bring great benefit to the development of photoredox radical-mediated reactions.

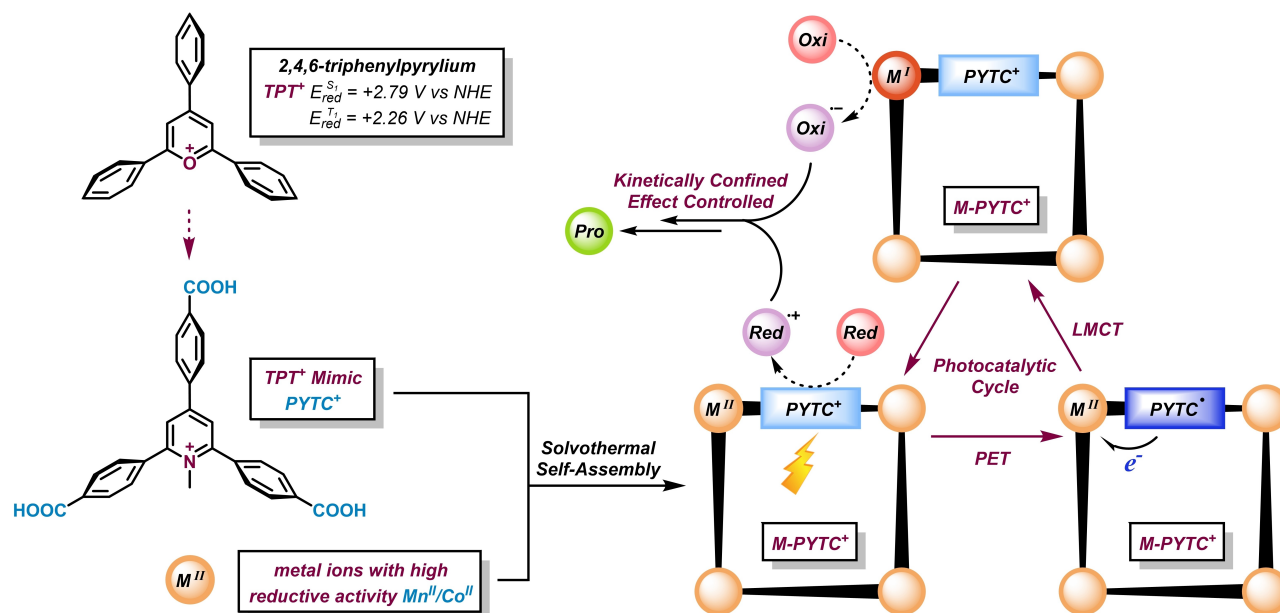
2,4,6-Triphenylpyrylium (TPT^+) functions as a classic organic photoredox catalyst, has a noteworthy absorption in the visible range, and is strongly oxidizing in both the singlet and triplet excited states [$E_{\text{red}}^{\text{S}_1} = +2.79$ V vs. NHE (normal hydrogen electrode); $E_{\text{red}}^{\text{T}_1} = +2.26$ V vs. NHE].^[3] However,

[*] Q. Zhang, Prof. Y. Jin, L. Ma, Y. Zhang, Prof. Dr. C. Meng, Prof. Dr. C. Duan
 State Key Laboratory of Fine Chemicals, Zhang Dayu School of Chemistry, Dalian University of Technology
 Dalian 116024 (China)
 E-mail: jinyh18@dlut.edu.cn
 cyduan@dlut.edu.cn

with the high oxidation potential in the excited state, the ground-state reduction potential of TPT^\bullet is not sufficiently negative to reduce $^3\text{O}_2$ to generate superoxide ($\text{O}_2^{\bullet-}$),^[11] which is the key step in most aerobic oxidation reactions. Furthermore, TPT^+ is not stable enough to exist with strong nucleophilic reagents.^[12] By turning the pyrylium into a stable pyridinium structure and equipping three coordinating carboxyl groups, herein, we design a TPT^+ mimic, 2,4,6-tris(4-carboxyphenyl)-1-methylpyridin-1-ium (PYTC^+) as an organic linker coordinated with metal ions possessing high reductive activity in the reduction state to construct a novel photoredox MOP platform (Scheme 1). Taking advantage of the spatial and kinetic confinement effects of MOPs, we envisioned that the photo-oxidative half reaction via photo-induced electron transfer (PET) and the reductive half reaction via metal catalysis can be restricted in the confined microenvironments and integrated through LMCT. As expected, the optical antenna PYTC^+ reaches its excited state $[\text{PYTC}^+]^*$ under visible-light irradiation, followed by a SET process with a reducing organic substrate to release a cationic radical intermediate $[\text{Red}]^{\bullet+}$ and $[\text{PYTC}]^\bullet$. An internal LMCT from $[\text{PYTC}]^\bullet$ to M^{II} gives M^{I} and the regeneration of the PYTC^+ photocatalyst. With the strong reducing capacity of M^{I} species, single-electron reduction with another oxidizing substrate is feasible, affording $[\text{Oxi}]^{\bullet-}$ and resetting the catalytic cycle. Rapid combination of $[\text{Red}]^{\bullet+}$ and $[\text{Oxi}]^{\bullet-}$ occurs to form the cross-coupling product controlled by the kinetically confined effect. To the best of our knowledge, this is the first dual-catalysed platform for photoredox radical-coupling reactions based on TPT^+ mimics, providing promise for the establishment and development of scalable and sustainable synthetic strategies.

Results and Discussion

The solvothermal reaction of $\text{MnCl}_2 \cdot 4\text{H}_2\text{O}$ and PYTC^+ in a mixed solvent of CH_3CN and N,N -dimethylformamide (DMF) at 120°C for 3 days afforded the TPT^+ -mimic-containing MOP (named as Mn-PYTC^+) in a high yield. Co-PYTC^+ was prepared in a similar way with $\text{Co}(\text{NO}_3)_2 \cdot 6\text{H}_2\text{O}$ and PYTC^+ in CH_3CN . Single-crystal X-ray diffraction (SCXRD) analysis revealed that both Mn-PYTC^+ and Co-PYTC^+ crystallise in a triclinic system (space group $P\bar{1}$) with $\text{M}_3(\text{COO})_6\text{X}_2$ ($\text{M}=\text{Mn}, \text{Co}$; $\text{X}=\text{Cl}, \text{NO}_3$) as the secondary building unit (SBU) (Table S1–S3). Furthermore, the coincidence of powder X-ray diffraction (PXRD) peaks between Mn-PYTC^+ and Co-PYTC^+ indicated that they are isomorphous (Figure S1). As shown in Figure 1a, the central atom Mn of the SBU in Mn-PYTC^+ is hexa-coordinated with six oxygen atoms from PYTC^+ ligands, exhibiting an octahedral geometry. The other two Mn atoms at terminal positions are penta-coordinated, featuring coordination by four oxygen atoms from PYTC^+ ligands and one axial Cl atom in a distorted trigonal-bipyramidal configuration. The metal–oxygen cluster in Co-PYTC^+ shows a similar coordination pattern except for the terminal Co atom hexa-coordinated by four oxygens from PYTC^+ and two from a nitrate instead of Cl (Figure 1b). M-PYTC^+ adopts a two-dimensional (2D) layered network with each trinuclear cluster SBU bridged by six carboxylate ligands (Figures 1c, S2–S4). π - π interactions between adjacent layers result in a staggered AB stacking fashion in M-PYTC^+ (Figures 1d, S5–S7), which is likely to facilitate the excitation delocalization and enhance the light-harvesting ability for the MOP.^[13] The purity of the as-synthesized crystals after desolvation treatment was verified by PXRD patterns that



Scheme 1. The building blocks and self-assembly process of MOP M-PYTC^+ , and the conceptual illustration for the synergistic photocatalytic platform merged with PET, LMCT, and radical couplings confined by spatial and kinetic effects. Oxi = oxidizing substrate, Red = reducing substrate, Pro = product.

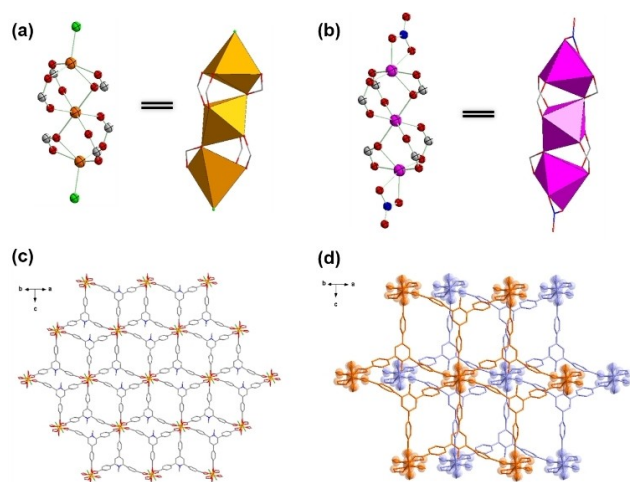


Figure 1. Coordination environment of trinuclear clusters in a) **Mn-PYTC⁺** and b) **Co-PYTC⁺**; c) the top view of the 2D network structure of **Mn-PYTC⁺**; d) the top view of the stacking model in **Mn-PYTC⁺**. All hydrogen atoms and solvent molecules are omitted for clarity, and branched chains are also omitted. Orange, Mn; pink, Co; red, O; blue, N; grey, C; green, Cl.^[37]

matched well with the simulated one for **M-PYTC⁺** (Figure S1). Scanning electron microscopy (SEM) and energy dispersive spectrometer (EDS) mapping images displayed that Mn, Cl, and N elements were uniformly distributed in the block crystal of **Mn-PYTC⁺** (Figure S8). The thermal stability of the two as-synthesized MOPs was investigated next. Thermogravimetric analysis (TGA) showed that both **Mn-PYTC⁺** and **Co-PYTC⁺** are thermally stable up to 300 °C (Figures S9–S10), ensuring the maintenance of the

framework structure during the catalytic reaction at room temperature.

The optical and electrical properties of **M-PYTC⁺** were studied next. The UV/Vis spectra of **Mn-PYTC⁺** and **Co-PYTC⁺** showed a broader absorption over the visible-light range than **PYTC⁺** (Figure 2a). The stacking π - π interactions between ligands and the distorting coordination geometry of metal centres in **M-PYTC⁺** are speculated to contribute to the red shift of the UV/Vis absorption band.^[14] The band gaps (E_g) of **Mn-PYTC⁺** and **Co-PYTC⁺** were estimated to be 2.86 and 3.10 eV, respectively, by the Kubelka–Munk (KM) method from Tauc plots (Figure 2d), demonstrating their application prospects as semiconducting photocatalysts.^[15] To further elucidate the semiconductor character and photocatalytic abilities of **M-PYTC⁺**, Mott–Schottky electrochemical measurements were performed at frequencies of 500, 1000, and 1500 Hz (Figures 2e and f). The positive slope of the linear plots demonstrates the typical *n*-type semiconducting character of **M-PYTC⁺**.^[16] The flat band positions determined from the intersection are -1.02 V vs. Ag/AgCl (i.e., -0.82 V vs. NHE) for **Mn-PYTC⁺** and -1.09 V vs. Ag/AgCl (i.e., -0.89 V vs. NHE) for **Co-PYTC⁺**. With the bottom of the conduction band (LUMO) in *n*-type semiconductors generally approximate to the flat-band potential,^[17] the LUMO of **Mn-PYTC⁺** is estimated to be -0.82 V vs. NHE, and the top of valence band (HOMO) is calculated to be 2.04 V vs. NHE. The LUMO and HOMO of **Co-PYTC⁺** are -0.89 V and 2.21 V vs. NHE. Similar results were also obtained via ultraviolet photoelectron spectroscopy (UPS) analysis on the ionization potentials (equivalent to valence band maximum, VBM) of **Mn-PYTC⁺** and **Co-PYTC⁺** (Figures S11–S12). The sufficiently positive potential of the HOMO and negative

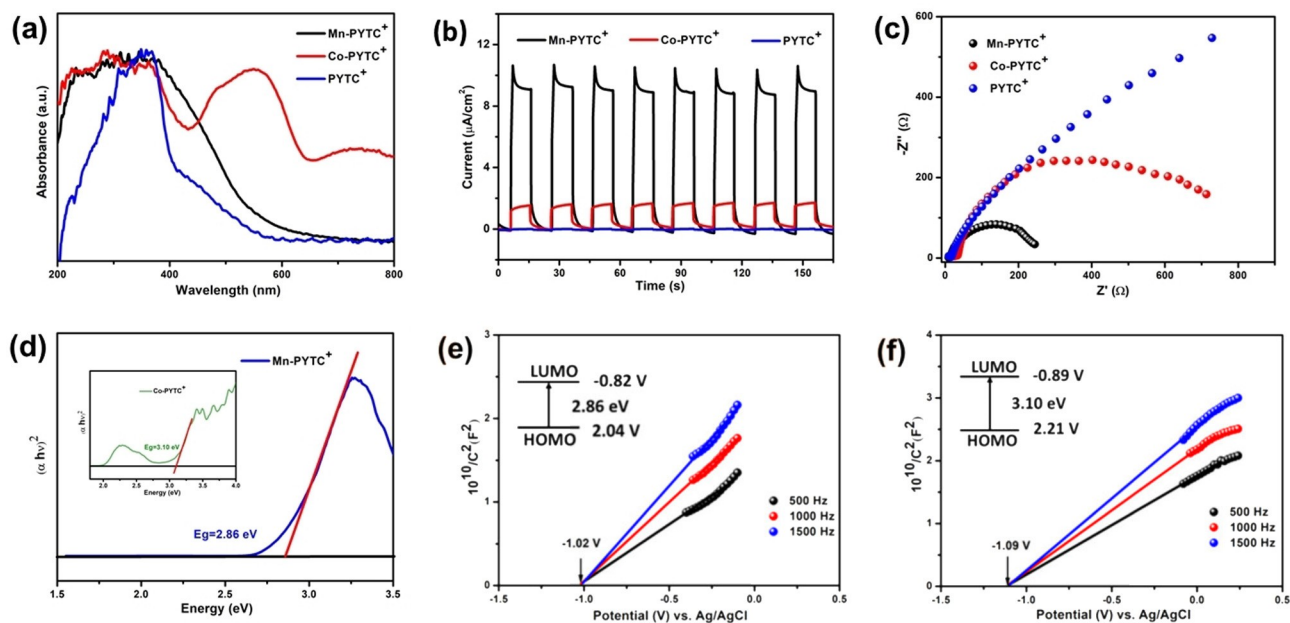


Figure 2. a) UV/Vis spectra, b) photocurrent responses, and c) EIS plots of **Mn-PYTC⁺**, **Co-PYTC⁺**, and **PYTC⁺**; d) Tauc plots of **Mn-PYTC⁺** and **Co-PYTC⁺**; e, f) Mott–Schottky plots for **Mn-PYTC⁺** and **Co-PYTC⁺**, respectively, in 0.1 M KCl aqueous solution (insets are the energy diagrams of HOMO and LUMO levels)

potential of the LUMO of both **Mn-PYTC**⁺ and **Co-PYTC**⁺ suggests a wide application in various photoinduced organic synthesis reactions. In view of the charge-separation efficiency of photocatalysts being an important influencing factor for photocatalytic processes, photocurrent, time-resolved fluorescence emission decay, and electrochemical impedance spectroscopy (EIS) experiments were then carried out for comparison. **Mn-PYTC**⁺ exhibits obviously stronger photocurrent responses than **Co-PYTC**⁺ and **PYTC**⁺ at different wavelengths (Figures 2b, S13–S14), implying that added free-charge carriers, which provide an efficient separation level for photogenerated electron-hole (*e-h*) pairs and an enhanced catalytic activity, are generated.^[18] The promoted charge-separation efficiency of **Mn-PYTC**⁺ was further confirmed by the shorter lifetime of the excited state when compared with **PYTC**⁺ (Figure S15).^[19] EIS for **Mn-PYTC**⁺ shows the smallest radius and lowest charge-transfer resistance (Figure 2c), suggesting the high efficiency for charge transfers in **Mn-PYTC**⁺.^[20]

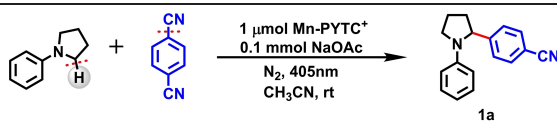
A typical challenging photoredox radical-coupling reaction, direct C(sp³)-H arylation of *N*-phenylpyrrolidine with 1,4-dicyanobenzene, was chosen as the model reaction to investigate the photocatalytic activities of **M-PYTC**⁺ (Table 1). After considerable effort, we found that the reaction presented the best result in the presence of **Mn-PYTC**⁺ and NaOAc under 405 nm LED irradiation at room temperature for 5 h, and was able to give the target product **1a** in a high isolated yield of 92 % (entry 1). The main peaks from the PXRD pattern of the as-synthesized **Mn-PYTC**⁺ remained after the reaction, certifying the integrity and stability of the MOP structure (Figure S17). Control experiments showed that both photocatalysts and light irradiation were crucial for the photoinduced arylation reaction (entries 2–3). Removing the inorganic base was detrimental to the yield of **1a** (entry 4). Importantly, no **1a** was obtained with a single active motif of MnCl₂·4H₂O or **PYTC**⁺, or a simple mix of

both as photocatalysts, verifying that synergistic catalysis and spatially confined electron transfer between metal nodes and organic ligands in **M-PYTC**⁺ (entries 5–7) were essential. By contrast, **Co-PYTC**⁺ only furnished the cross-coupling product in a 30 % yield under the same conditions, consistent with the results from the photocurrent and EIS experiments (entry 8). Dimethylacetamide (DMAC) was another effective solvent for the model reaction, realizing the complete conversion of substrates in 1 h. However, the isolated yield of **1a** only reached 86 % with undesirable formation of some unknown by-products (entry 9). Further investigation on the effect of light wavelengths showed the reaction efficiency for **M-PYTC**⁺ decreased obviously with wavelength extension (Figure S18).

α -Arylated amines, as a classic kind of high-value-added structure, have widespread applications in the pharmaceutical industry, such as producing therapeutic drugs and bioactive compounds.^[21] Thus, it is of great benefit to expand the substrate scope for the efficient C(sp³)-H arylation of amines via heterogeneous photocatalysis. As shown in Table 2, various cyanobenzenes with different electron-withdrawing groups were surveyed first as radical precursors with C-CN bond cleavage, giving the desired arylated amines in satisfying yields (**1a–1e**). Additional amines, including *N*-phenylpiperidine and *N*-phenylmorpholine, also exhibited good activities in this strategy with DMAC instead of CH₃CN as the solvent (**1f–1g**). Compared to the previously reported results with the Ir-catalysed homogeneous system,^[22] the reaction time was markedly shortened without obvious loss of yield. Moreover, multifluoroarenes and multisubstituted monofluoroalkenes are fundamental structural motifs in medicinal chemistry and agrochemistry.^[23] Applying our photocatalytic platform, these valuable building blocks could also be synthesized with gem-difluorostyrenes and aryl donors Ar_F-F as substrates. After a slight adjustment in reaction conditions, the α -amino C(sp³)-H multifluoroarylation (**1h–1j**) and monofluoroalkenylation (**1k–1m**) of amines were also achieved with moderate-to-good efficiency with **Mn-PYTC**⁺ as the photocatalyst.

To explore the detailed electron-transfer processes in photocatalysis, Stern-Volmer fluorescence quenching experiments were employed. Among the substrates and Mn²⁺ species contained in the catalytic system, only *N*-phenylpyrrolidine could quench the fluorescence of **PYTC**⁺ near 430 nm (Figures S19–S22). Based on the free energy change (*E*_{0,0}) between the ground and vibrationally relaxed excited states, the oxidation potential *E*_{red}(**P***/**P**^{•+}) of the excited-state **PYTC**⁺ was determined as +2.73 V vs. NHE, which is similar to that of **TPT**⁺ (Figure S16 and Table S4).^[3] Both the fluorescence-quenching results and the high oxidation potential demonstrated that an SET process occurred between photoexcited [**PYTC**⁺]^{*} and *N*-phenylpyrrolidine (*E*_{red} = +0.95 V vs. NHE)^[22] to start the catalytic cycle. Impressively, the fluorescence intensity of **PYTC**⁺ attenuated by a strong electron donor, triethylamine, could be partially recovered with the addition of MnCl₂·4H₂O (Figures S23–S24). This phenomenon implied the intermediate [**PYTC**][•] was capable of transferring a single electron to

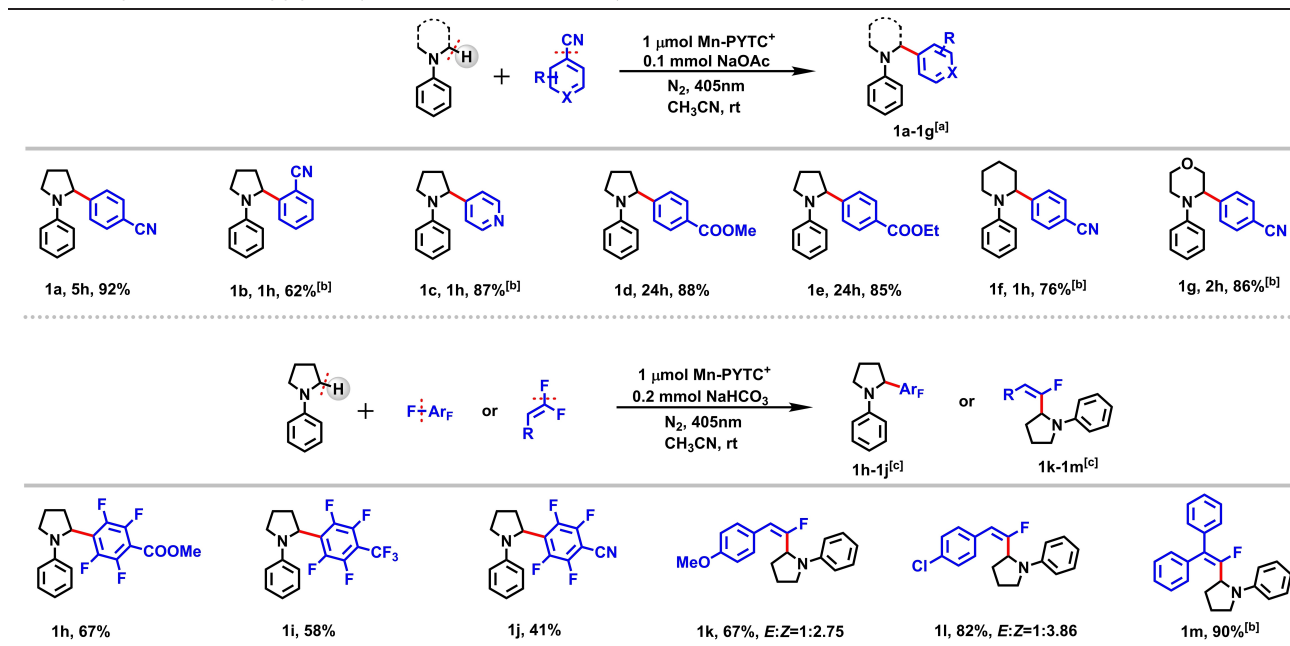
Table 1: Control experiments of reaction conditions.^[a]



Entry	Deviation from standard conditions	Yield (1a) [%]
1	None	92
2	Without Mn-PYTC ⁺	trace
3	Without light	0
4	Without NaOAc	34
5 ^[b]	MnCl ₂ ·4H ₂ O instead of Mn-PYTC ⁺	trace
6 ^[c]	PYTC ⁺ instead of Mn-PYTC ⁺	0
7 ^[b,c]	MnCl ₂ ·4H ₂ O + PYTC ⁺ instead of Mn-PYTC ⁺	0
8	Co-PYTC ⁺ instead of Mn-PYTC ⁺	30
9	DMAC instead of CH ₃ CN	86 (1 h)

[a] Standard conditions: amine (0.2 mmol), 1,4-dicyanobenzene (0.1 mmol), NaOAc (0.1 mmol), **Mn-PYTC**⁺ (1 μmol, 0.01 equiv) in CH₃CN (1 mL) irradiated with a 30 W 405 nm LED at room temperature for 5 h. Yields were determined as isolated product.

[b] 3 μmol MnCl₂·4H₂O. [c] 3 μmol **PYTC**⁺.

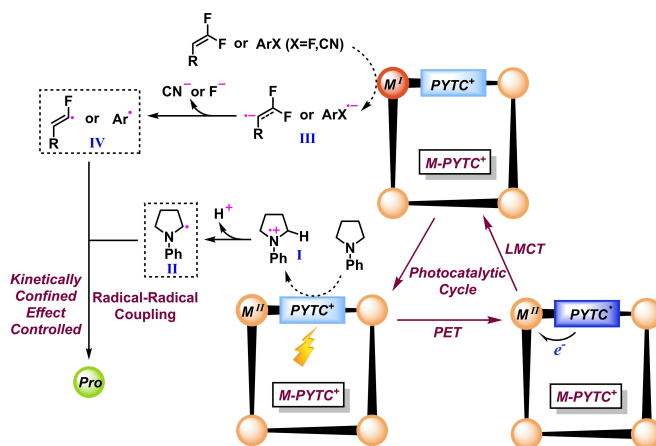
Table 2: Scope of α -amino C(sp³)-H arylation and monofluoroalkenylation of amines.

[a] Reaction conditions: amine (0.2 mmol), benzonitrile (0.1 mmol), NaOAc (0.1 mmol), **Mn-PYTC**⁺ (1 μ mol, 0.01 equiv) in CH₃CN (1 mL) irradiated with a 30 W 405 nm LED at room temperature. Yields were determined as isolated product. [b] DMAC instead of CH₃CN. [c] Amine (0.2 mmol), fluorobenzene or gem-difluoroalkenes (0.1 mmol), NaHCO₃ (0.2 mmol), **Mn-PYTC**⁺ (1 μ mol, 0.01 equiv) in CH₃CN (1 mL) irradiated with a 30 W 405 nm LED at room temperature for 24 h. Yields were determined as isolated product. The E/Z values were determined by ¹H NMR spectroscopy.

the metal node in some cases. Meanwhile, no similar trend was observed with (2,2-difluoroethene-1,1-diyl)dibenzene as the recovering reagent, eliminating the possibility of the direct SET from **[PYTC]**[•] to the oxidizing substrate (Figure S25). Quenching experiments were performed next (Table S5). The cross-coupling reaction was completely inhibited by addition of excess 2,2,6,6-tetramethylpiperidinoxy (TEMPO) or 2,6-di-tert-butyl-4-methylphenol (BHT), suggesting the reaction undergoes a radical pathway (entries 1 and 2).^[24] KI and AgNO₃, respectively as hole and electron scavengers, also induced an entire loss of reaction efficiency, implying that both holes and electrons played important roles in this photoredox system (entries 3 and 4).^[25]

Based on the above results and the model electron-transfer system shown in Scheme 1, we proposed a reaction mechanism for α -amino C(sp³)-H arylation and monofluoroalkenylation of amines (Scheme 2). Under irradiation by visible light, the photoexcited **[PYTC]**^{•+} is easily engaged in a SET process with *N*-phenylpyrrolidine to release ground-state **[PYTC]**[•] and radical **I**. Deprotonation of **I** delivers α -amino radical **II**.^[26] Meanwhile, M(I) generated by the subsequent LMCT is able to reduce the radical precursor to form an anionic radical intermediate **III**, followed by cleavage of a C-F^[23] or C-CN^[22] bond to provide another carbon radical **IV**. Eventually, kinetic-confinement-effect-controlled radical-radical combination between radical **II** and **IV** furnishes the desired product.

Encouraged by the fantastic catalytic activities of our **Mn-PYTC**⁺ photoredox platform, we next turned our

**Scheme 2.** Proposed mechanisms for α -amino C(sp³)-H arylation and monofluoroalkenylation of amines.

attention to the aerobic oxidative coupling reaction of benzylamines as a probe reaction consisting of an organic coupling reaction and molecular oxygen activation. After systematic optimization, the model reaction showed the best efficiency under the standard conditions as shown in Table S6, entry 1. As the reaction time prolonged, benzaldehyde was detected as a by-product during the aerobic coupling reaction, suggesting that the reaction time should be precisely controlled for acquiring the pure target product. Benzylamine was hardly converted into **2a** under N₂ instead of an air atmosphere, indicating that O₂ was indispensable

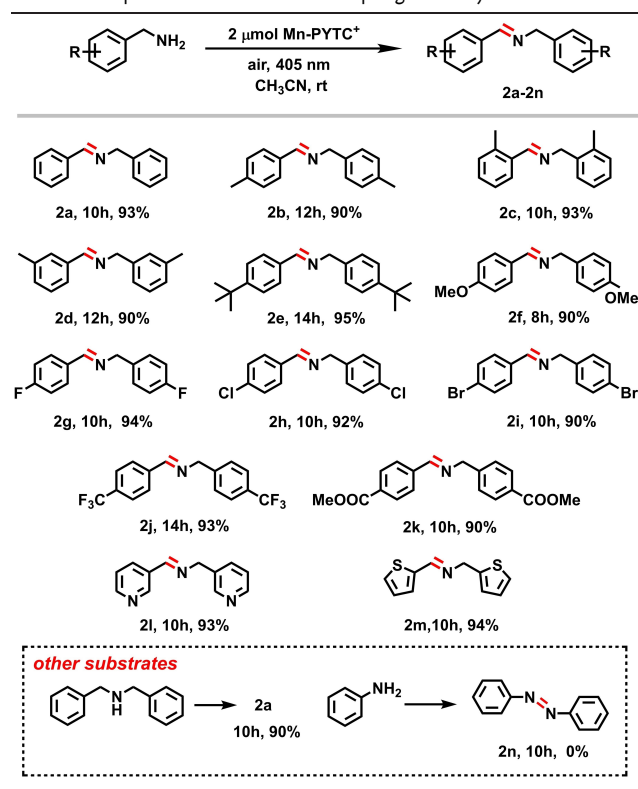
for the oxidative reaction (entries 2 and 3). No coupling product was observed in the absence of light or photocatalyst, proving the transformation from benzylamine to *N*-benzylbenzaldimine to be assuredly driven by **Mn-PYTC**⁺ photocatalysis (entries 4 and 5). In addition, **2a** could not be produced in abundance when using $\text{MnCl}_2 \cdot 4\text{H}_2\text{O}$ or **PYTC**⁺ as photocatalysts (entries 6–7). Replacement of **Mn-PYTC**⁺ with **Co-PYTC**⁺ resulted in slightly reduced activity, giving an 88% conversion rate of benzylamine under the same conditions (entry 8).

Considering that two processes, radical couplings and O_2 activation, are involved in the probe reaction, we conducted a series of photocatalytic experiments on **Mn-PYTC**⁺ based on the oxidation of benzylamine. A time-course study of **Mn-PYTC**⁺ photocatalysis showed the conversion of benzylamine increasing in a linear fashion (Figure S26), revealing a pseudo-zero-order kinetic behavior. To explore the heterogeneous catalysis nature, **Mn-PYTC**⁺ was filtered out after 6 h and consequently no more product was obtained even after extending the reaction time to 10 h (Figure S27). The stability and recyclability of **Mn-PYTC**⁺ were subsequently examined and its activity was well maintained in five continuous cycles (Figure S28). Also, there was no marked difference between the recovered and as-synthesized PXRD patterns, confirming the structural integrity and stability of **Mn-PYTC**⁺ during the catalytic reaction (Figure S29).

The substrate scope of selective benzylamine oxidation was investigated to demonstrate the general applicability (Table 3) of the reaction. Benzylamines substituted with various electron-donating and electron-withdrawing groups were transformed into their corresponding products in excellent yields (**2a–2k**). Heterocyclic amines, such as pyridin-3-ylmethanamine and 2-thiophenemethylamine, known as poisons to metal catalysts,^[27] were also examined and displayed satisfying yields (**2l–2m**). Secondary dibenzylamine afforded the target product **2a** smoothly with a similar comparable yield. However, aniline without a hydrogen atom at its α -carbon was not a suitable substrate for the oxidative coupling (**2n**), suggesting that a hydrogen abstraction process might be indispensable in this reaction.

Additional exploratory experiments were performed to further inspect the mechanism of electron-transfer and oxygen-activation courses. Firstly, fluorescence-quenching outcomes showed that the emission of photoexcited **PYTC**⁺ was quenched by benzylamine (Figures S30–S31), emerging a similar SET process between the bridging ligand and benzylamine ($E_{\text{red}} \approx +1.47 \text{ V vs. NHE}$).^[10a] Importantly, the fluorescence-recovery phenomenon was also obtained with the subsequent addition of $\text{MnCl}_2 \cdot 4\text{H}_2\text{O}$ after benzylamine, further proving the internal LMCT process from [**PYTC**]⁺ to the metal node (Figure S32). Moreover, inspired by the previous studies,^[28] molecular oxygen species are converted into reactive oxygen species (ROS) via SET or EnT with photosensitizers. When the singlet oxygen ($^1\text{O}_2$) scavenger, 9,10-diphenylanthracene (DPA), was added into the reaction under standard conditions, the endoperoxide generated by DPA and $^1\text{O}_2$ was successfully detected by high resolution mass spectra (HRMS), uncovering the involvement of $^1\text{O}_2$ in the photocatalytic system (Figure S33).^[29]

Table 3: Scope of aerobic oxidative coupling of benzylamines.^[a]



[a] Reaction conditions: benzylamine (0.2 mmol), **Mn-PYTC**⁺ (2 μmol , 0.01 equiv) in CH_3CN (2 mL) irradiated with a 30 W 405 nm LED at room temperature under air atmosphere. Yields were determined by ^1H NMR spectroscopy by using mesitylene as an internal standard.

Additionally, 2,2,6,6-tetramethylpiperidine (TEMP) was employed as the $^1\text{O}_2$ trapping agent to further confirm the $^1\text{O}_2$ formation by electron-spin-resonance (ESR) spectroscopy, and a typical triplet peak for TEMP was observed under long-time visible-light irradiation (Figure 3a).^[30] Replacing TEMP with 5,5-dimethyl-1-pyrroline *N*-oxide (DMPO) as the $\text{O}_2^{\bullet-}$ and $\bullet\text{OH}$ radical trapping agent, a specific sextet signal attributed to $\text{DMPO-O}_2^{\bullet-}$, but no obvious signal for $\bullet\text{OH}$, was collected sensitively by ESR spectra in situ, confirming the quick generation of $\text{O}_2^{\bullet-}$ (Figure 3b).^[28b] Deep insights into the key roles of ROS in the oxidative coupling of amines were obtained by quenching experiments (Table S7). Introducing tert-butanol, the representative inhibitor for $\bullet\text{OH}$,^[10a] into the model reaction had little effect on the conversion of benzylamine, further excluding the formation of the hydroxyl radical (entry 2). 1,4-diazabicyclo-[2.2.2]octane (DABCO), which can eliminate $^1\text{O}_2$,^[31] only inhibited the reaction to a certain extent (entry 3). In contrast, the amount of **2a** was greatly reduced when benzoquinone (BQ) as an $\text{O}_2^{\bullet-}$ inhibitor^[10a] was used (entry 4). Both ESR and quenching experiments showed that $\text{O}_2^{\bullet-}$ plays a more vital role than $^1\text{O}_2$ in the photo-mediated aerobic oxidation of amines. The surmised reason is that the electron donors quench [**PYTC**]⁺* via SET several orders of magnitude faster than $^3\text{O}_2$ via EnT, which is similar to the characteristic of **TPT**⁺.^[11] Finally, the

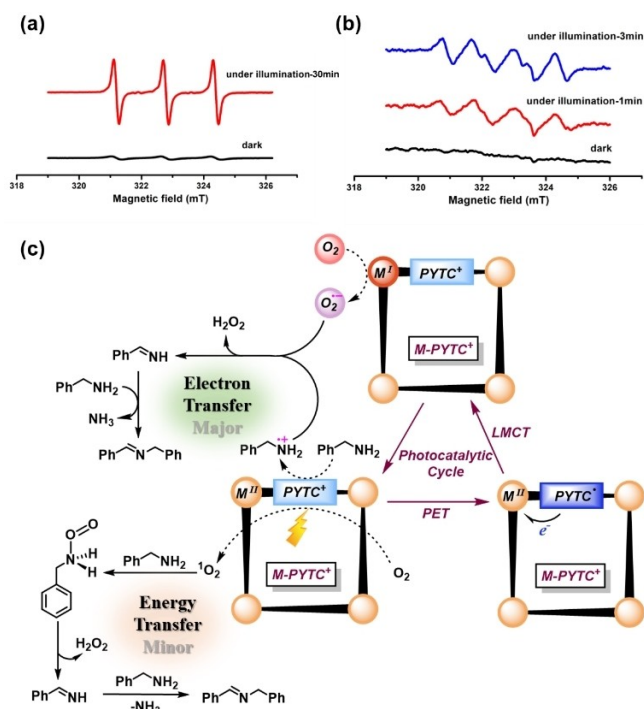


Figure 3. a) ESR detection of $^1\text{O}_2$ generation with Mn-PYTC⁺ trapped by TEMP. b) ESR detection of $\text{O}_2^{\bullet-}$ generation with Mn-PYTC⁺ trapped by DMPO. c) Proposed mechanism for the photocatalytic molecular oxygen activation and aerobic oxidative coupling of benzylamine catalysed by Mn-PYTC⁺: superoxide radical anion (electron transfer) and singlet oxygen (energy transfer) pathways.

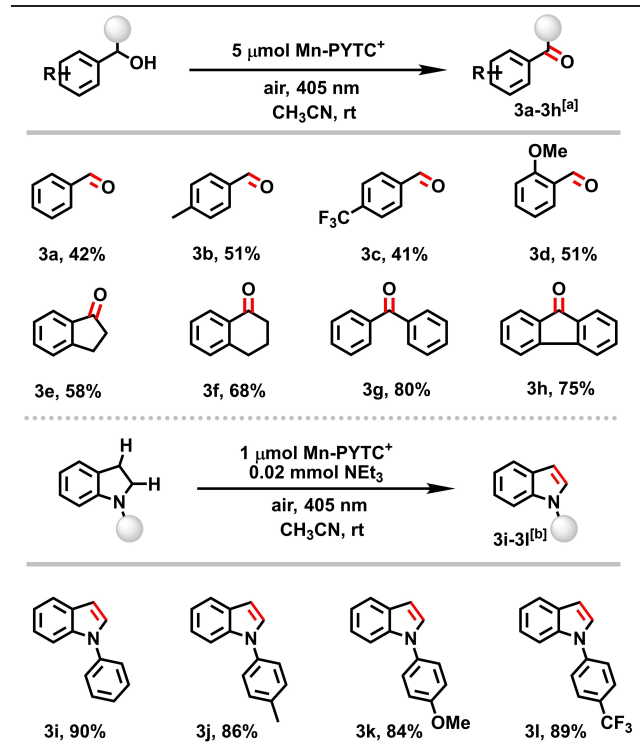
decreased yields induced by TEMPO and BHT certified the inclusion of radical processes (entries 5 and 6).^[24]

According to the above investigations and reported literatures, a plausible mechanism for aerobic oxidative coupling of amines was proposed (Figure 3c). Initially, a PET between excited [PYTC⁺]* and benzylamine gives a cationic radical PhCH₂NH₂^{•+} and a reducing species. A subsequent LMCT from [PYTC⁺]* to metal node Mn^{II} offers Mn^I and regenerates PYTC⁺. Mn^I can effectively realise molecular oxygen activation to achieve active O₂^{•-}. Afterwards, the produced O₂^{•-} abstracts a proton and a hydrogen atom from PhCH₂NH₂^{•+}, affording the corresponding intermediate imine. A cross-coupling between imine and another benzylamine supplies the target product with removal of ammonia.^[27] Meanwhile, a small amount of product is acquired through an EnT-induced ¹O₂ pathway that can directly oxidise amines to imines.^[32]

Photocatalysed oxidation of alcohols to the corresponding carbonyl products has a great significance in the pharmaceutical and commodity industries.^[33] Traditional catalytic protocols are mainly based on Ru and Pd species with high temperature, leading to extra economic and environmental burdens.^[34] Enlightened by the desirable property of Mn-PYTC⁺ for photoactivation of molecular oxygen species, we extended the applicability of our platform to the selective benzylic C(sp³)-H oxidation of alcohols to aromatic carbonyl derivatives with O₂ as the only oxidant. Control experiments unfolded the necessity of light, catalyst,

and O₂ (Table S8, entries 1–5). As shown in Table 4, Mn-PYTC⁺ displayed good catalytic activities on the oxidation of various primary and secondary benzylic alcohols under mild reaction conditions with a broad substrate scope and good functional-group tolerance (3a–3h). Stern–Volmer quenching investigations revealed that benzyl alcohol is qualified for quenching the emission of photoexcited PYTC⁺ (Figures S34, S35). On the basis of experiments and previous reports,^[35] we concluded that the excited photocatalyst first oxidises benzyl alcohol to provide a cationic radical intermediate, followed by hydrogen-atom abstraction and deprotonation induced by a superoxide radical to generate the carbonyl product (Figure S36).^[6b] This aerobic oxidation strategy could also be applied to the catalytic synthesis of indole derivatives, which are important structural motifs in natural products and pharmaceuticals.^[36] Under an air atmosphere and with visible-light irradiation, diverse N-substituted indoles with different functional groups were achieved in high yields via oxidative dehydrogenation of indolines catalysed by Mn-PYTC⁺ (Table 4, 3i–3l).

Table 4: Scope of oxidative dehydrogenation of alcohols and indolines.



[a] Reaction conditions: benzyl alcohol (0.1 mmol), Mn-PYTC⁺ (5 μmol, 0.05 equiv) in CH₃CN (1 mL) irradiated with a 30 W 405 nm LED at room temperature under air atmosphere for 24 h. Yields were determined by ¹H NMR spectroscopy by using 1,3,5-trimethoxybenzene (0.05 mmol) as an internal standard. [b] Indoline (0.1 mmol), Mn-PYTC⁺ (1 μmol, 0.01 equiv), Et₃N (0.02 mmol, 0.2 equiv) in CH₃CN (2 mL) irradiated with a 30 W 405 nm LED at room temperature under air atmosphere for 1 h. Yields were determined by ¹H NMR spectroscopy by using 1,3,5-trimethoxybenzene (0.05 mmol) as an internal standard.

Conclusion

In summary, we have developed a novel photoredox MOP platform assembled by **TPT**⁺-mimic ligands as organic linkers and reductive metal ions as nodes, integrating photo-induced electron transfer, ligand-to-metal charge transfer, and molecular oxygen activation events for synergistic catalysis. The desirable photocatalytic performances of **Mn-PYTC**⁺ in synthesis, including α -amino C(sp³)-H arylation and monofluoroalkenylation of amines via cleavage of C-F or C-CN bonds, aerobic oxidative coupling of benzylamines, and selective dehydrogenation oxidation of alcohols and indolines, demonstrate that the spatial and kinetic confinement effects of the structurally confined microenvironments of MOPs result in an improvement in the efficiency of continuous electron transfers and radical-radical couplings. We believe that this work will provide inspiration for the design of photocatalytic and enzymatic simulation tactics with metal-organic supramolecular systems.

Acknowledgements

We highly appreciate Dr. Haijun Yang and Dr. Xianjin Zhu at Tsinghua University for their great help with ESR experiments. We highly appreciate Dr. Na Li, Dr. Hao Wang and Dr. Huarong Tong at Nankai University, and Dr. Hao Xu at Henan University for their great help with UPS experiments. We acknowledge the support of the National Natural Science Foundation of China (21901032, 21890381, 21820102001) and the Fundamental Research Funds for the Central Universities (DUT21LK13).

Conflict of Interest

The authors declare no conflict of interest.

Data Availability Statement

The data that support the findings of this study are available in the Supporting Information of this article.

Keywords: Confinement Effect • Metal-Organic Polymers • O₂ Activation • Organic Couplings • Photocatalysis

- [1] a) D. M. Schultz, T. P. Yoon, *Science* **2014**, *343*, 1239176; b) M. D. Käarkäs, J. A. Porco, Jr., C. R. Stephenson, *Chem. Rev.* **2016**, *116*, 9683–9747; c) C. K. Prier, D. A. Rankic, D. W. MacMillan, *Chem. Rev.* **2013**, *113*, 5322–5363; d) D. M. Yan, J. R. Chen, W. J. Xiao, *Angew. Chem. Int. Ed.* **2019**, *58*, 378–380; *Angew. Chem.* **2019**, *131*, 384–386.
- [2] L. Marzo, S. K. Pagire, O. Reiser, B. König, *Angew. Chem. Int. Ed.* **2018**, *57*, 10034–10072; *Angew. Chem.* **2018**, *130*, 10188–10228.
- [3] N. A. Romero, D. A. Nicewicz, *Chem. Rev.* **2016**, *116*, 10075–10166.

- [4] J. I. Day, K. Teegardin, J. Weaver, J. Chan, *Org. Process Res. Dev.* **2016**, *20*, 1156–1163.
- [5] a) J. Twilton, C. Le, P. Zhang, M. H. Shaw, R. W. Evans, D. W. C. MacMillan, *Nat. Chem. Rev.* **2017**, *1*, 0052; b) L. Buzzetti, G. E. M. Crisenza, P. Melchiorre, *Angew. Chem. Int. Ed.* **2019**, *58*, 3730–3747; *Angew. Chem.* **2019**, *131*, 3768–3786.
- [6] a) T. P. Yoon, M. A. Ischay, J. Du, *Nat. Chem.* **2010**, *2*, 527–532; b) J. M. R. Narayanan, C. R. J. Stephenson, *Chem. Soc. Rev.* **2011**, *40*, 102–113.
- [7] a) K. L. Skubi, T. R. Blum, T. P. Yoon, *Chem. Rev.* **2016**, *116*, 10035–10074; b) H.-P. Deng, Q. Zhou, J. Wu, *Angew. Chem. Int. Ed.* **2018**, *57*, 12661–12665; *Angew. Chem.* **2018**, *130*, 12843–12847.
- [8] a) C. D. Windle, R. N. Perutz, *Coord. Chem. Rev.* **2012**, *256*, 2562–2570; b) F. Li, Y. Jiang, B. Zhang, F. Huang, Y. Gao, L. Sun, *Angew. Chem. Int. Ed.* **2012**, *51*, 2417–2420; *Angew. Chem.* **2012**, *124*, 2467–2470; c) L. Zeng, X. Guo, C. He, C. Duan, *ACS Catal.* **2016**, *6*, 7935–7947; d) W. K. Haug, E. M. Moscarello, E. R. Wolfson, P. L. McGrier, *Chem. Soc. Rev.* **2020**, *49*, 839–864; e) C. Liu, K. Liu, C. Wang, H. Liu, H. Wang, H. Su, X. Li, B. Chen, J. Jiang, *Nat. Commun.* **2020**, *11*, 1047; f) X. Zhang, M. C. Wasson, M. Shayan, E. K. Berdichevsky, J. Ricardo-Noordberg, Z. Singh, E. K. Papazyan, A. J. Castro, P. Marino, Z. Ajoyan, Z. Chen, T. Islamoglu, A. J. Howarth, Y. Liu, M. B. Majewski, M. J. Katz, J. E. Mondloch, O. K. Farha, *Coord. Chem. Rev.* **2021**, *429*, 213615; g) Y. Chen, P. Li, J. Zhou, C. T. Buru, L. Dordevic, P. Li, X. Zhang, M. M. Cetin, J. F. Stoddart, S. I. Stupp, M. R. Wasielewski, O. K. Farha, *J. Am. Chem. Soc.* **2020**, *142*, 1768–1773; h) J. Baek, B. Rungtaweeworanit, X. Pei, M. Park, S. C. Fakra, Y. S. Liu, R. Matheu, S. A. Alshimri, S. Alshihri, C. A. Trickett, G. A. Somorjai, O. M. Yaghi, *J. Am. Chem. Soc.* **2018**, *140*, 18208–18216.
- [9] a) X. P. Wu, L. Gagliardi, D. G. Truhlar, *J. Am. Chem. Soc.* **2018**, *140*, 7904–7912; b) J.-L. Wang, C. Wang, W. Lin, *ACS Catal.* **2012**, *2*, 2630–2640; c) Y. Y. Zhu, G. Lan, Y. Fan, S. S. Veroneau, Y. Song, D. Micheroni, W. Lin, *Angew. Chem. Int. Ed.* **2018**, *57*, 14090–14094; *Angew. Chem.* **2018**, *130*, 14286–14290; d) L. Zeng, T. Liu, C. He, D. Shi, F. Zhang, C. Duan, *J. Am. Chem. Soc.* **2016**, *138*, 3958–3961; e) P. Cai, M. Xu, S. S. Meng, Z. Lin, T. Yan, H. F. Drake, P. Zhang, J. Pang, Z. Y. Gu, H. C. Zhou, *Angew. Chem. Int. Ed.* **2021**, *60*, 27258–27263; *Angew. Chem.* **2021**, *133*, 27464–27469; f) M. Ding, R. W. Flaig, H. L. Jiang, O. M. Yaghi, *Chem. Soc. Rev.* **2019**, *48*, 2783–2828; g) Q. Xia, Z. Li, C. Tan, Y. Liu, W. Gong, Y. Cui, *J. Am. Chem. Soc.* **2017**, *139*, 8259–8266.
- [10] a) C. Xu, H. Liu, D. Li, J. H. Su, H. L. Jiang, *Chem. Sci.* **2018**, *9*, 3152–3158; b) Y. Jin, Q. Zhang, Y. Zhang, C. Duan, *Chem. Soc. Rev.* **2020**, *49*, 5561–5600; c) L. Zhang, G. Ng, N. Kapoor-Kaushik, X. Shi, N. Corrigan, R. Webster, K. Jung, C. Boyer, *Angew. Chem. Int. Ed.* **2021**, *60*, 22664–22671; *Angew. Chem.* **2021**, *133*, 22846–22853; d) J. K. Jin, K. Wu, X. Y. Liu, G. Q. Huang, Y. L. Huang, D. Luo, M. Xie, Y. Zhao, W. Lu, X. P. Zhou, J. He, D. Li, *J. Am. Chem. Soc.* **2021**, *143*, 21340–21349; e) Y. Fan, E. You, Z. Xu, W. Lin, *J. Am. Chem. Soc.* **2021**, *143*, 18871–18876; f) Y. Pan, Y. Qian, X. Zheng, S. Q. Chu, Y. Yang, C. Ding, X. Wang, S. H. Yu, H. L. Jiang, *Natl. Sci. Rev.* **2021**, *8*, nwa224; g) B. Guo, X. Cheng, Y. Tang, W. Guo, S. Deng, L. Wu, X. Fu, *Angew. Chem. Int. Ed.* **2022**, *61*, e202117244; *Angew. Chem.* **2022**, *134*, e202117244; h) C. Zhang, C. Xie, Y. Gao, X. Tao, C. Ding, F. Fan, H.-L. Jiang, *Angew. Chem. Int. Ed.* **2022**, <https://doi.org/10.1002/anie.202204108>; *Angew. Chem.* **2022**, <https://doi.org/10.1002/ange.202204108>; i) J. Y. Zeng, X. S. Wang, B. R. Xie, Q. R. Li, X. Z. Zhang, *J. Am. Chem. Soc.* **2022**, *144*, 1218–1231; j) S. Naghdi, A. Cherevan, A. Giesriegl, R. Guillet-Nicolas, S. Biswas, T.

- Gupta, J. Wang, T. Haunold, B. C. Bayer, G. Rupprechter, M. C. Toroker, F. Kleitz, D. Eder, *Nat. Commun.* **2022**, *13*, 282.
- [11] R. Akaba, H. Sakuragi, K. Tokumaru, *J. Chem. Soc. Perkin Trans. 2* **1991**, 291–297.
- [12] U. Gruntz, A. R. Katritzky, D. H. Kenny, M. C. Rezende, H. Sheikh, *J. Chem. Soc. Chem. Commun.* **1977**, 701–701.
- [13] T. Zhang, X. Guo, Y. Shi, C. He, C. Duan, *Nat. Commun.* **2018**, *9*, 4024.
- [14] H. Li, Y. Yang, X. Jing, C. He, C. Duan, *Chem. Sci.* **2021**, *12*, 8512–8520.
- [15] a) N. Li, J. Liu, J. J. Liu, L. Z. Dong, Z. F. Xin, Y. L. Teng, Y. Q. Lan, *Angew. Chem. Int. Ed.* **2019**, *58*, 5226–5231; *Angew. Chem.* **2019**, *131*, 5280–5285; b) X.-K. Wang, J. Liu, L. Zhang, L.-Z. Dong, S.-L. Li, Y.-H. Kan, D.-S. Li, Y.-Q. Lan, *ACS Catal.* **2019**, *9*, 1726–1732; c) D. Shi, R. Zheng, M. J. Sun, X. Cao, C. X. Sun, C. J. Cui, C. S. Liu, J. Zhao, M. Du, *Angew. Chem. Int. Ed.* **2017**, *56*, 14637–14641; *Angew. Chem.* **2017**, *129*, 14829–14833.
- [16] a) J. S. Qin, S. Yuan, L. Zhang, B. Li, D. Y. Du, N. Huang, W. Guan, H. F. Drake, J. Pang, Y. Q. Lan, A. Alsalmeh, H. C. Zhou, *J. Am. Chem. Soc.* **2019**, *141*, 2054–2060; b) J. Zhou, Y. Wang, Z. Cui, Y. Hu, X. Hao, Y. Wang, Z. Zou, *Appl. Catal. B* **2020**, *277*, 119228; c) H. Q. Xu, J. Hu, D. Wang, Z. Li, Q. Zhang, Y. Luo, S. H. Yu, H. L. Jiang, *J. Am. Chem. Soc.* **2015**, *137*, 13440–13443.
- [17] a) K. Maeda, K. Sekizawa, O. Ishitani, *Chem. Commun.* **2013**, *49*, 10127–10129; b) Z. Zhang, J. Long, L. Yang, W. Chen, W. Dai, X. Fu, X. Wang, *Chem. Sci.* **2011**, *2*, 1826–1830.
- [18] T. Song, L. Zhang, P. Zhang, J. Zeng, T. Wang, A. Ali, H. Zeng, *J. Mater. Chem. A* **2017**, *5*, 6013–6018.
- [19] Z. B. Fang, T. T. Liu, J. Liu, S. Jin, X. P. Wu, X. Q. Gong, K. Wang, Q. Yin, T. F. Liu, R. Cao, H. C. Zhou, *J. Am. Chem. Soc.* **2020**, *142*, 12515–12523.
- [20] X. Fang, Q. Shang, Y. Wang, L. Jiao, T. Yao, Y. Li, Q. Zhang, Y. Luo, H. L. Jiang, *Adv. Mater.* **2018**, *30*, 1705112.
- [21] J. Xie, M. Rudolph, F. Rominger, A. S. K. Hashmi, *Angew. Chem. Int. Ed.* **2017**, *56*, 7266–7270; *Angew. Chem.* **2017**, *129*, 7372–7376.
- [22] A. McNally, C. K. Prier, D. W. C. MacMillan, *Science* **2011**, *334*, 1114–1117.
- [23] C.-L. Cao, G.-X. Zhang, F. Xue, H.-P. Deng, *Org. Chem. Front.* **2022**, *9*, 959–965.
- [24] a) Y. Jin, L. Ou, H. Yang, H. Fu, *J. Am. Chem. Soc.* **2017**, *139*, 14237–14243; b) Y. Jin, Q. Zhang, L. Wang, X. Wang, C. Meng, C. Duan, *Green Chem.* **2021**, *23*, 6984–6989.
- [25] R. Garg, S. Mondal, L. Sahoo, C. P. Vinod, U. K. Gautam, *ACS Appl. Mater. Interfaces* **2020**, *12*, 29324–29334.
- [26] G. W. Dombrowski, J. P. Dinnocenzo, P. A. Zielinski, S. Farid, Z. M. Wosinska, I. R. Gould, *J. Org. Chem.* **2005**, *70*, 3791–3800.
- [27] F. Raza, J. H. Park, H.-R. Lee, H.-I. Kim, S.-J. Jeon, J.-H. Kim, *ACS Catal.* **2016**, *6*, 2754–2759.
- [28] a) A. A. Ghogare, A. Greer, *Chem. Rev.* **2016**, *116*, 9994–10034; b) S. Yang, X. Li, Y. Qin, Y. Cheng, W. Fan, X. Lang, L. Zheng, Q. Cao, *ACS Appl. Mater. Interfaces* **2021**, *13*, 29471–29481.
- [29] R. Sun, X. Yang, Y. Ge, J. Song, X. Zheng, M. Yuan, R. Li, H. Chen, H. Fu, *ACS Catal.* **2021**, *11*, 11762–11773.
- [30] M. Cao, S. Wang, J. H. Hu, B. H. Lu, Q. Y. Wang, S. Q. Zang, *Adv. Sci.* **2022**, *9*, 2103721.
- [31] M. Klaper, T. Linker, *J. Am. Chem. Soc.* **2015**, *137*, 13744–13747.
- [32] J. A. Johnson, J. Luo, X. Zhang, Y.-S. Chen, M. D. Morton, E. Echeverría, F. E. Torres, J. Zhang, *ACS Catal.* **2015**, *5*, 5283–5291.
- [33] D. Muñoz Solano, P. Hoyos, M. J. Hernáiz, A. R. Alcántara, J. M. Sánchez-Montero, *Bioresour. Technol.* **2012**, *115*, 196–207.
- [34] T. Mallat, A. Baiker, *Chem. Rev.* **2004**, *104*, 3037–3058.
- [35] G. Ji, L. Zhao, J. Wei, J. Cai, C. He, Z. Du, W. Cai, C. Duan, *Angew. Chem. Int. Ed.* **2022**, *61*, e202114490; *Angew. Chem.* **2022**, *134*, e202114490.
- [36] S. W. Youn, T. Y. Ko, *Asian J. Org. Chem.* **2018**, *7*, 1467–1487.
- [37] Deposition Numbers 2125267 (for **Mn-PYTC⁺**), 2125268 (for **Co-PYTC⁺**) contains the supplementary crystallographic data for this paper. These data are provided free of charge by the joint Cambridge Crystallographic Data Centre and Fachinformationszentrum Karlsruhe Access Structures service.

Manuscript received: April 4, 2022

Accepted manuscript online: June 3, 2022

Version of record online: July 8, 2022